Neuron
NeuroResource

Mapping Sensory Circuits by Anterograde Transsynaptic Transfer of Recombinant Rabies Virus

Niccolò Zampieri,[1] Thomas M. Jessell,[1,*] and Andrew J. Murray[1]
[1]Departments of Neuroscience and Biochemistry and Molecular Biophysics, Howard Hughes Medical Institute, Kavli Institute for Brain Science, Columbia University, New York, NY 10032 USA
*Correspondence: tmj1@columbia.edu
http://dx.doi.org/10.1016/j.neuron.2013.12.033

SUMMARY

Primary sensory neurons convey information from the external world to relay circuits within the CNS, but the identity and organization of the neurons that process incoming sensory information remains sketchy. Within the CNS, viral tracing techniques that rely on retrograde transsynaptic transfer provide a powerful tool for delineating circuit organization. Viral tracing of the circuits engaged by primary sensory neurons has, however, been hampered by the absence of a genetically tractable anterograde transfer system. In this study, we demonstrate that rabies virus can infect sensory neurons in the somatosensory system, is subject to anterograde transsynaptic transfer from primary sensory to spinal target neurons, and can delineate output connectivity with third-order neurons. Anterograde transsynaptic transfer is a feature shared by other classes of primary sensory neurons, permitting the identification and potentially the manipulation of neural circuits processing sensory feedback within the mammalian CNS.

INTRODUCTION

Primary sensory neurons serve as the sole neural conduit through which signals from the external world are transmitted to circuits within the CNS. Sensory neurons in the dorsal root ganglia (DRG) convey somatosensory information about temperature, touch, muscle activation, and limb position to second-order neurons in the spinal cord, but the basic logic through which functional subclasses of DRG neurons engage spinal circuits remains poorly defined. Only in the case of the monosynaptic stretch reflex circuit constructed from the connections of group Ia proprioceptive sensory neurons and target motor neurons is there clarity about precise patterns of sensory input connectivity and their links to behavior (Brown, 1981). Defining the spinal targets of discrete populations of peripheral sensory neurons could help to resolve how somatosensory information is processed at primary relay stations within the CNS.

Transsynaptic tracing has proven to be an effective means of mapping neural connections. Plant lectins such as wheat germ agglutinin and barley lectin are transferred from sensory to recipient neurons in both vertebrates and invertebrates but at low efficiency and in unmodifiable form (Braz et al., 2002; Horowitz et al., 1999; Boehm et al., 2005). Neurotropic viruses of the herpes simplex virus (HSV) family have been used as tracers that permit the transfer of genetic material to sensory-recipient neurons, offering the possibility of neuronal visualization and manipulation (Mata et al., 2002). However, neither lectins nor HSV transfer can be easily restricted to first-order recipient neurons, undermining their utility in circuit mapping. Within the mammalian CNS, rabies virus (RV) has gained prominence as a reliable transsynaptic tracer and its versatility for recombinant engineering permits the restriction of transsynaptic transfer to first-order recipient neurons (Wickersham et al., 2007a, 2007b). RV appears to exhibit broad CNS neurotropism, a selective retrograde route of transfer, and comparatively limited neurotoxicity (Ugolini, 2008, 2010). Together, these features have permitted the mapping of presynaptic inputs to several defined populations of CNS neurons (Callaway, 2008; Ugolini, 2011).

At first glance, two of the major attributes of RV biology in the mapping of CNS circuits appear to preclude its use as an effective transsynaptic tracer for primary sensory neurons. First, it remains unclear if, and how effectively, RV can infect primary sensory neurons (Ugolini, 2010, 2011). Second, the selective retrograde transfer of RV is at odds with the anterograde route required to map sensory-recipient neurons. Nevertheless, there are reports of RV infection of certain classes of primary sensory neurons and the subsequent spread to CNS neurons (Lafay et al., 1991; Astic et al., 1993). In particular, wild-type RV has been reported to infect neurons in the DRG, under conditions in which spread to spinal target neurons has been detected (Velandia-Romero et al., 2013). Given these preliminary accounts it may be worth considering the possibility that the traditional view of central RV tropism and rigid retrograde transfer breaks down in the context of primary sensory neurons.

In this study, we have addressed two main issues: can recombinant RV efficiently infect primary sensory neurons conveying different functional modalities and, if so, can it spread transsynaptically in the anterograde direction to map the identity, distribution, and target connectivity of sensory-recipient CNS neurons? We show that RV infects sensory neuron subtypes in the somatosensory, vestibular, and olfactory systems without

obvious restriction in tropism. In addition, we demonstrate selective anterograde transsynaptic transfer of recombinant RV from defined sensory populations to molecularly identified recipient neurons. Finally, we document how anterograde RV tracing can permit high-resolution mapping of the input-output organization of sensory-recipient neurons. Thus, RV can be used to trace the central connectivity of diverse classes of primary sensory neurons, permitting a systematic approach to the identification and manipulation of circuits involved in the initial processing of sensory signals.

RESULTS

Infection and Anterograde Transsynaptic Transfer of RV from DRG Neurons

To test whether RV can infect sensory neurons in mouse DRG, we injected the glycoprotein (G)-deficient attenuated SAD-B19 RV strain encoding GFP (Wickersham et al., 2007a, 2010) (RVΔG-GFP) into the gastrocnemius (GS) or tibialis anterior (TA) muscles of neonatal mice. We focused on these ankle extensor (GS) and flexor (TA) muscles because detailed accounts of the wiring of their sensory-motor reflex arcs are available (Burke and Tsairis, 1973; Stephens et al., 1975; Burke et al., 1977).

We observed GFP expression in DRG neurons 3 days after injection of RVΔG-GFP into the GS muscle, and the number of infected neurons attained steady state after 6 days (Figure S1 available online; data not shown). We examined whether different functional subclasses of DRG neurons are susceptible to RV infection. To address this issue, we analyzed the coexpression of RV-transduced GFP with molecular markers of sensory neuron subtype, focusing on nociceptor ($TrkA^+$) and proprioceptor ($PV^+/Rx3^+$) identities (Marmigère and Ernfors, 2007). In wild-type mice injected intramuscularly with RVΔG-GFP, we detected an ~5-fold greater incidence of $GFP^+/TrkA^+$ than $GFP^+/PV^+/Rx3^+$ neurons, in keeping with the ~6-fold greater incidence of $TrkA^+$ neurons over $PV^+/Rx3^+$ in DRG neurons at lumbar level 3 to 6 (Figure S1). Thus, hindlimb injection of RV infects DRG sensory neuron subtypes with similar incidence. To estimate the efficiency with which RV infects proprioceptive sensory neurons after muscle injection, we assumed that each of the ~19 intrafusal muscle spindles found in the GS reflects the presence of two or three proprioceptors (one group Ia and one or two group II) and that each of the ~19 Golgi-tendon organs (GTOs) is innervated by a single group Ib proprioceptor (Figure S1; see Supplemental Experimental Procedures for muscle spindle and GTO counts). Based on these numbers, we estimate that ~12% of all proprioceptive neurons innervating the GS muscles were infected with RV.

We examined whether recombinant RV can be transferred anterogradely from proprioceptor terminals into sensory-recipient spinal neurons, focusing first on patterns of connectivity between proprioceptors and motor neurons (Eccles et al., 1957). Since muscle injection of SAD-B19 RV results in direct infection of both sensory and motor neurons (Figure S1), we set out to restrict viral infection to sensory neurons by preparing a pseudotyped RV with predefined tropism. The endogenous RV coat was substituted with the avian sarcoma/leucosis virus subtype A envelope (EnvA, RVΔG-GFP-EnvA), which restricts RV infection to cells expressing the avian TVA receptor (Wickersham et al., 2007b). To achieve cellular specificity of the TVA receptor, we used a conditional transgenic mouse line in which expression of rabies virus glycoprotein (RV-G) and TVA is under the control of cre-recombinase (Figures 1A and 1B; referred to as RGT; Takatoh et al., 2013). We introduced one of two cre lines: advillin-cre (*Avil::cre*), which directs transgene expression to all DRG neurons (da Silva et al., 2011), and parvalbumin-cre (*PV::cre*), which preferentially targets proprioceptive sensory neurons and a small subset of low-threshold cutaneous mechanoreceptors (Hippenmeyer et al., 2007; de Nooij et al., 2013).

Consistent with the patterns of endogenous advillin and parvalbumin expression, we observed that RV-G was expressed in all DRG neurons and excluded from spinal neurons in *Avil::cre*$^{+/-}$; *RGT*$^{+/-}$ mice (Figure 1C), whereas in *PV::cre*$^{+/-}$; *RGT*$^{+/-}$ mice RV-G was confined to only ~10% of all sensory neurons (Figure 1F). We used a floxed reporter line to confirm that *Avil::cre* and *PV::cre* direct specific transgene expression in DRG but not in motor neurons (Figure S2). Muscle injection of RVΔG-GFP-EnvA in *PV::cre*$^{+/-}$; *RGT*$^{+/-}$ mice resulted in restricted expression of GFP in PV^+ sensory neurons, whereas injection in *Avil::cre*$^{+/-}$; *RGT*$^{+/-}$ mice resulted in a broader expression of GFP in the DRG (Figure S1; data not shown). GFP expression was not detected in the DRG or spinal cord after muscle injection of RVΔG-GFP-EnvA in *RGT*$^{+/-}$ mice in the absence of a cre driver line, confirming the tight transcriptional control of TVA expression (Figure S2). Thus, TVA expression restricts primary infection of EnvA-pseudotyped RV to predefined sensory neuron subtypes.

These findings allowed us to examine whether complementation of RV-G in sensory neurons permits transsynaptic viral transfer into spinal motor neurons. To assess this, we injected RVΔG-GFP-EnvA into the GS muscle in *Avil::cre*$^{+/-}$; *RGT*$^{+/-}$ or *PV::cre*$^{+/-}$; *RGT*$^{+/-}$ mice. Six days after injection, we detected GFP expression in a subset of motor neurons, located in a dorsal/medial position of the lateral motor column (LMC) at lumbar levels 3 and 4, consistent with the stereotypic location of the GS motor pool (Figures 1D, 1E, 1G, and 1H and Figure S3; McHanwell and Biscoe, 1981). We did not detect GFP expression in the median motor column (MMC) or in preganglionic (PGC) neurons, an indication that proprioceptive sensory neurons supplying limb muscles form preferential connections with LMC motor neurons (Figures 1E and 1H and Figure S3).

We examined the efficiency of motor neuron labeling achieved by anterograde sensory transfer. After GS injection in *Avil::cre*$^{+/-}$; *RGT*$^{+/-}$ mice, we detected GFP expression in ~30% of all motor neurons of the posterior crural columel (those innervating the GS, soleus, plantaris, tibialis posterior, flexor digitorum longus, and flexor hallucis longus muscles; McHanwell and Biscoe, 1981). In contrast, in *PV::cre*$^{+/-}$; *RGT*$^{+/-}$ mice, we detected GFP expression only in ~10% of posterior crural motor neurons, suggesting a lower efficiency of cre-recombination. Motor neuron labeling was also obtained after RV injection into the TA muscle (data not shown). Thus, RV appears capable of efficient anterograde transsynaptic transfer from DRG neurons to spinal motor neurons.

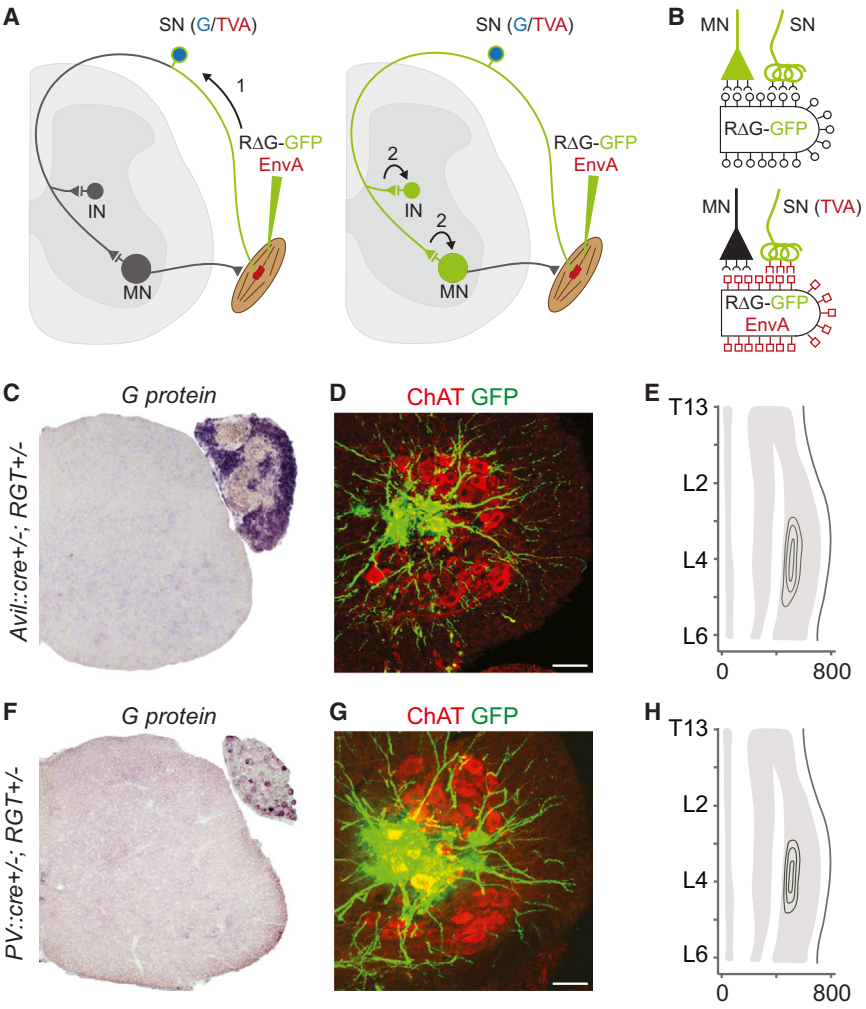

Figure 1. RV Infection of DRG Neurons and Anterograde Transfer to Spinal Targets

(A) Selective primary infection of sensory neurons using the EnvA/TVA system (left). RV-G complementation in sensory neurons allows RV-ΔG monosynaptic transfer in the anterograde direction to secondary targets in the spinal cord (right).

(B) RV infection of motor neurons and sensory neurons (top); selective sensory neuron infection after pseudotyping RV with EnvA and expression of the TVA receptor in sensory neurons (bottom).

(C and F) RV-G mRNA expression in all sensory neurons in *Avil::cre*$^{+/-}$; *RGT*$^{+/-}$ mice (C) and in a subset of sensory neurons in *PV::cre*$^{+/-}$; *RGT*$^{+/-}$ mice (F).

(D and G) RV monosynaptic labeling of motor neurons at lumbar level 3 (L3) of the spinal cord after RVΔG-GFP-EnvA injection in the GS muscle of *Avil::cre*$^{+/-}$; *RGT*$^{+/-}$ mice (D) and *PV::cre*$^{+/-}$; *RGT*$^{+/-}$ mice (G).

(E and H) Contour density analysis of motor neuron distribution from T13 to L6 levels in the longitudinal plane of the spinal cord after RVΔG-GFP-EnvA injections in the GS muscle of *Avil::cre*$^{+/-}$; *RGT*$^{+/-}$ mice (E; n = 3) and *PV::cre*$^{+/-}$; *RGT*$^{+/-}$ mice (H; n = 7). Gray areas represent cumulative positions of ChAT^{+} neurons. Coordinates on the x axis are distance in micrometers relative to the midline. Scale bars in (D) and (G) represent 50 μm. To see related data examining motor and sensory neuron infection by RV, see Figures S1, S2, and S3.

Sensory-Motor Connectivity Revealed by Anterograde RV Transsynaptic Transfer

We relied on the known precision of sensory-motor connections to examine the specificity of anterograde transsynaptic transfer of RV into motor neurons. We first determined whether motor neuron labeling occurs purely by transfer of RV from sensory neurons or by direct infection of motor axon terminals. Proprioceptive sensory neurons supplying muscle spindles provide monosynaptic input to alpha (α) but not gamma (γ) motor neurons (Figures 2A and 2B; Eccles et al., 1957, 1960). Thus, adventitious infection of RV in motor neurons should result in GFP expression in both α and γ motor neurons, whereas RV transfer via a sensory route should result in selective labeling of α motor neurons (Figures 2E and 2J).

We identified α motor neurons by their large cell body cross-sectional area (>400 μm^2), expression of NeuN, and exclusion of Err3 (Figures 2B–2D; Friese et al., 2009; Ashrafi et al., 2012). In contrast, γ motor neurons were identified by their small cross-sectional area (<400 μm^2), expression of Err3, and exclusion of NeuN (Figures 2B–2D; Friese et al., 2009; Ashrafi et al., 2012). As a control, injection of RVΔG-GFP into the GS muscle of wild-type or *RGT*$^{+/-}$ control mice resulted in efficient GFP labeling of large Err3^{low}/NeuN^{high} α and small Err3^{high}/NeuN^{low} γ motor neurons (Figures 2E–2I), an indication that RV can infect both classes of motor neurons after intramuscular injection. To examine the selectivity of RV transsynaptic transfer via the sensory route, we injected RVΔG-GFP-EnvA into the GS muscle of *PV::cre*$^{+/-}$; *RGT*$^{+/-}$ mice. We detected selective GFP labeling of large diameter, Err3^{low}/NeuN^{high} α motor neurons, but not of γ motor neurons (Figures 2J–2N). This finding provides evidence that RV transfer occurs exclusively through a sensory route and results in selective transsynaptic infection of sensory-recipient neurons.

We next explored the organization of reflex arcs controlling the ankle joint to determine the feasibility of mapping sensory-motor circuits through anterograde transsynaptic transfer of RV. The lateral gastrocnemius (LG) and medial gastrocnemius (MG) muscles exert synergistic ankle extensor functions, whereas the TA muscle functions as an ankle flexor (Figure 3A; Eccles and Lundberg, 1958; Mendelson and Frank, 1991). Heteronymous motor neurons have been reported to make ~3-fold fewer group Ia sensory terminals than their homonymous counterparts (Nelson and Mendell, 1978). To label motor neurons that receive monosynaptic input from LG proprioceptors, we injected RVΔG-GFP-EnvA into the LG muscle of *Avil::cre*$^{+/-}$; *RGT*$^{+/-}$ mice (Figures 3B and 3C). Concurrently, we identified motor neurons supplying the synergist MG muscle through retrograde labeling of motor neurons after muscle injection of cholera toxin B

(CTB)^{A555} (Figures 3B and 3C). Many GFP$^+$ motor neurons were detected in positions coincident with the known location of LG motor neurons (Figures 3D–3I; McHanwell and Biscoe, 1981). In addition, GFP expression was detected in ~20% of CTB^{A555+} MG neurons, an indication that these motor neurons receive heteronymous connections from LG sensory neurons (Figures 3D–3F).

We tested the specificity of anterograde sensory transfer by examining whether TA motor neurons, which do not receive direct LG proprioceptive input, were infected after RV injection. We injected RVΔG-GFP-EnvA into the LG muscle of *Avil::cre*$^{+/-}$; *RGT*$^{+/-}$ mice and identified motor neurons supplying the antagonist TA muscle through concurrent TA muscle injection of CTB^{A647} (Figure 3B). Many GFP-labeled motor neurons were detected at L3 levels, but GFP expression in CTB^{A647} TA motor neurons was never observed (Figures 3G–3I). Thus, recombinant RV appears to promote synaptically constrained anterograde transsynaptic labeling of motor neurons from proprioceptors.

The labeling of motor neurons suggests that RV can transfer in the anterograde direction via axodendritic/axosomatic synapses. We therefore addressed whether RV can also transfer via axoaxonic synapses, examining a subpopulation of GABAergic interneurons responsible for presynaptic inhibition of proprioceptive neurons (Betley et al., 2009; Figure S4). This subset of inhibitory interneurons, referred to as GABApre neurons, is defined by expression of the GABA synthetic enzyme GAD2 that accumulates in presynaptic boutons juxtaposed with proprioceptive terminals on motor neurons (Betley et al., 2009; Figure S4). Thus, we analyzed GFP labeling of GAD2 boutons after RVΔG-GFP-EnvA muscle injection in *PV::cre* $^{+/-}$; *RGT*$^{+/-}$ animals. We found many examples of GFP-labeled GAD2 boutons in the ventral horn of the spinal cord, supporting the idea that RV may be capable of transfer to GABApre interneurons through axoaxonic synapses (Figure S4).

Sensory-Recipient Interneurons Revealed by Anterograde RV Transsynaptic Transfer

We next assessed whether anterograde RV tracing could also be used to map sensory-recipient interneuron populations in the spinal cord. We first analyzed the position of GFP-labeled interneurons in *Avil::cre*$^{+/-}$; *RGT*$^{+/-}$ mice in which RVΔG-GFP-EnvA had been injected into the GS muscle. We detected many GFP-labeled interneurons and found that 87% were located ipsilateral to the injected limb along much of the dorsoventral extent of the spinal cord. We also detected two small contralateral neuronal populations, one dorsal to the central canal (1.5% of labeled interneurons) and one ventral (11.7% of labeled interneurons; Figures 4A and 4B). Contralateral labeling of interneurons could reflect midline crossing of sensory afferents or of interneuron dendrites (Smith, 1983, 1986). We noted that only ~4% of labeled interneurons were located in the superficial dorsal horn (see Supplemental Experimental Procedures), a sparseness that is somewhat at odds with the representative labeling of TrkA$^+$ sensory neurons that innervate this domain (Figure S1). These findings could indicate either that RV is not efficiently transferred transsynaptically from small diameter C and Aδ fibers or that RV focal muscle injection limits the infection of cutaneous sensory neurons.

We also surveyed the distribution and identity of interneurons that receive monosynaptic input from PV$^+$ sensory afferents. After RVΔG-GFP-EnvA injection into the GS muscle of *PV::cre*$^{+/-}$; *RGT*$^{+/-}$ mice, we observed a more limited profile of interneuron labeling than in *Avil::cre*$^{+/-}$; *RGT*$^{+/-}$ animals (Figures 4C and 4D). We found that 98% of infected interneurons were located ipsilaterally, within the intermediate and ventral spinal cord (Figures 4C and 4D), indicating a more restricted engagement of interneurons by proprioceptors.

We next examined whether it is feasible to delineate the molecular identity of sensory-recipient interneurons infected with RV. To assess this, we analyzed the expression of FoxP2, Chx10, and Lhx1: transcription factors that mark a subpopulation of V1, V2a, and a collection of V0 and dI4 interneuron subtypes at both embryonic and postnatal stages (Figure 4E; Morikawa et al., 2009; Al-Mosawie et al., 2007; Pillai et al., 2007). After RVΔG-GFP-EnvA injection into the GS muscle of *PV::cre*$^{+/-}$; *RGT*$^{+/-}$ mice, we detected GFP expression in FoxP2$^+$ V1 interneurons, Chx10$^+$ V2a interneurons, and dorsal Lhx1$^+$ interneurons (Figures 4F–4H). Thus, molecularly defined subpopulations of interneurons can be identified after anterograde transsynaptic RV tracing.

Defining the Input-Output Connectivity of Sensory-Recipient Interneurons

We examined the possibility that anterograde transsynaptic transfer from primary sensory neurons provides a way of defining the output connectivity of sensory-recipient neurons. We noted that after RVΔG-GFP-EnvA injection in *PV::cre*$^{+/-}$; *RGT*$^{+/-}$ mice, GFP was expressed by a small set of cholinergic interneurons positioned close to the central canal, which we identified as V0$_C$ interneurons (Figures 5A and 5B; Zagoraiou et al., 2009). Since the principal output of V0$_C$ interneurons is via large cholinergic (C) boutons that contact the cell body and proximal dendrites of motor neurons (Zagoraiou et al., 2009), we tested the ability of sensory-transferred RV to delineate the synaptic terminals of this set of sensory-recipient interneurons. After RVΔG-GFP-EnvA infection in *PV::cre*$^{+/-}$; *RGT*$^{+/-}$ mice, we detected many GFP-labeled C boutons that contacted motor neuron somata (Figure 5C). Thus, in this instance, and likely more generally, RV-mediated anterograde transsynaptic transfer into sensory-recipient interneurons permits the simultaneous identification of the synaptic terminals and target output of labeled neurons.

Anatomical and physiological studies have pointed to a lack of direct proprioceptor input to V0$_C$ interneurons (Zagoraiou et al., 2009; Witts et al., 2014), prompting us to examine the relevant source of sensory input implied by our anterograde sensory transfer studies. At a transcriptional level, V0$_C$ interneurons are defined by expression of the homeodomain protein Pitx2 (Zagoraiou et al., 2009), and we therefore used a *Pitx2::cre* mouse line to direct RV infection and retrograde transsynaptic tracing from these neurons (Figure 5D). Injection of RVΔG-GFP-EnvA into the spinal cord of *Pitx2::cre* $^{+/-}$; *RGT* $^{+/-}$ mice resulted in GFP expression in V0$_C$ neurons, spinal interneurons, and DRG neurons (Figures 5E–5H). We found that ~70% of GFP$^+$ DRG neurons expressed the nociceptive marker TrkA and ~10% expressed PV, but we never

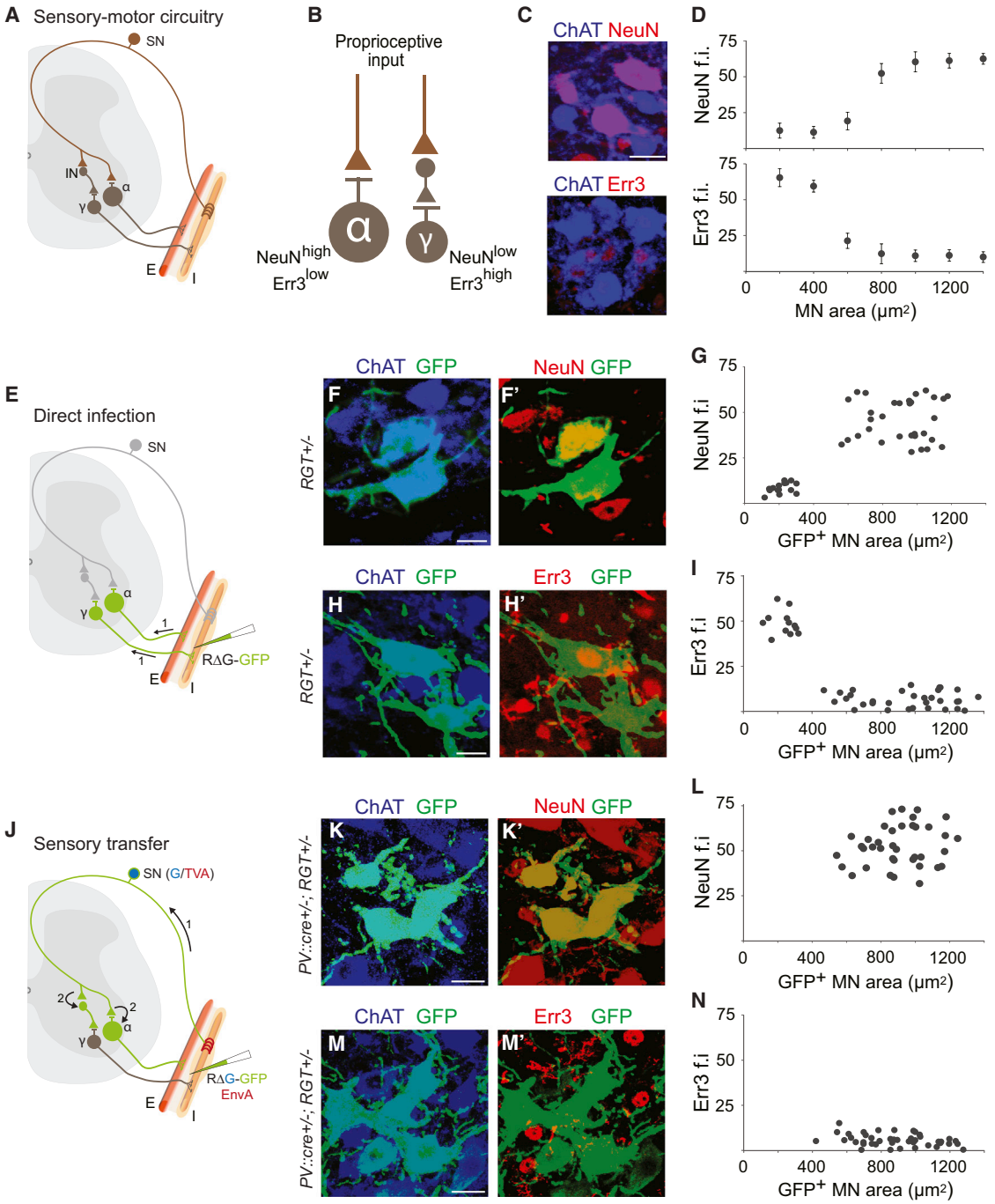

Figure 2. Specificity of RV Anterograde Transfer

(A) Schematic depicting proprioceptive sensory neuron innervation of α, but not γ, motor neurons (E, extrafusal muscle fibers; I, intrafusal muscle fibers).
(B) Molecular and anatomical distinctions between α and γ motor neurons.
(C) Representative images of α motor neurons expressing NeuN (top) or γ motor neurons expressing Err3 (bottom).
(D) Expression levels of NeuN (top) or Err3 (bottom) as a function of motor neuron soma area.
(E) Schematic of RVΔG-GFP muscle injection resulting in direct infection of both α and γ motor neurons.
(F and F′) ChAT and NeuN expression status in GFP^+ motor neurons.
(G) Quantitation of NeuN levels and motor neuron soma area after RVΔG-GFP muscle injection.
(H and H′) ChAT and Err3 expression status in GFP^+ motor neurons.
(I) Quantitation of Err3 levels and motor neuron soma area after RV-ΔG-GFP muscle injection.
(J) Schematic depicting muscle injection of RVΔG-GFP-EnvA of *PV::cre*$^{+/-}$; *RGT*$^{+/-}$ animals. Selective infection of sensory neurons and anterograde transsynaptic transport will result in secondary infection of α, but not γ, motor neurons.

(legend continued on next page)

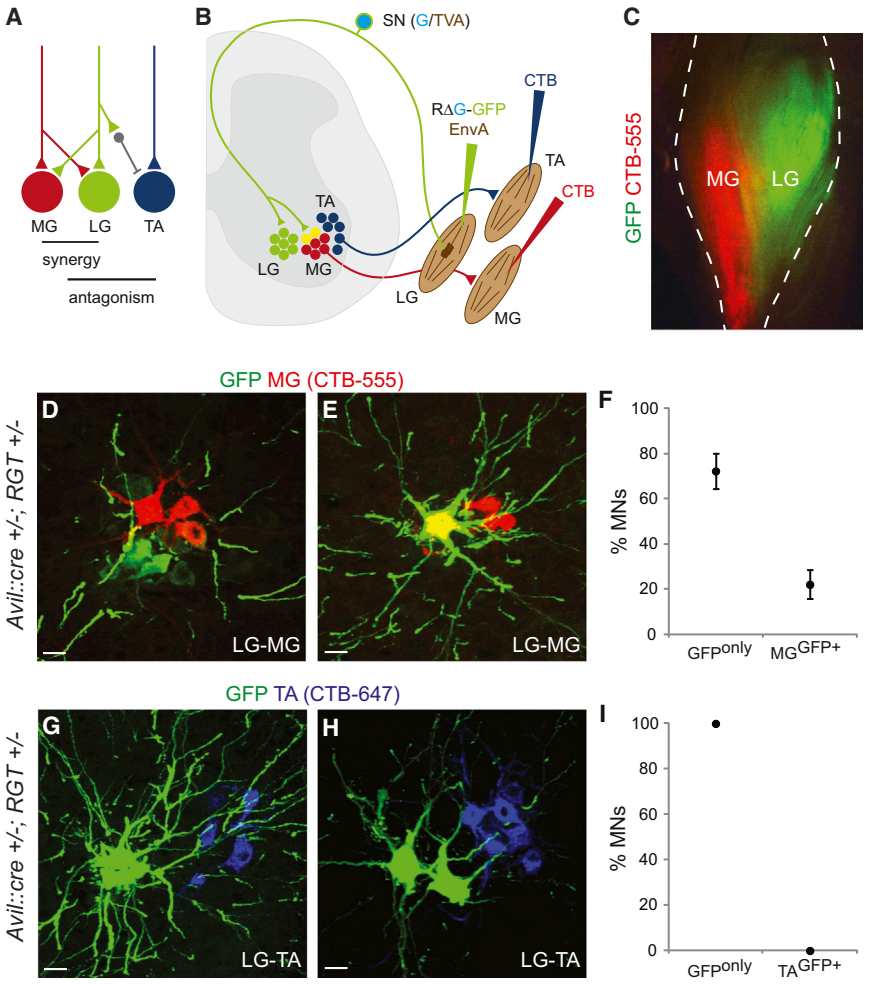

Figure 3. RV Anterograde Transfer Reveals the Organization of Sensory-Motor Reflex Arcs

(A) Basic organization of sensory-motor reflex arcs controlling the movement of the ankle joint.

(B) Experimental design to probe patterns of sensory motor connections using RV.

(C) Dorsal view of a mouse shank after MG (CTB-555) and LG (RVΔG-GFP-EnvA) muscle injections.

(D) Representative image of MG motor neurons retrogradely labeled by injection of CTB-555 into the MG muscle and motor neurons transsynaptically labeled after RVΔG-GFP-EnvA injection into the LG muscle of *Avil::cre*$^{+/-}$; *RGT*$^{+/-}$ *mice*.

(E) Example of an MG motor neuron receiving input from LG sensory afferents (CTB-555^{+}/GFP^{+}).

(F) Percentage of MG motor neurons transsynaptically labeled after RVΔG-GFP-EnvA injection into the LG muscle of *Avil::cre*$^{+/-}$; *RGT*$^{+/-}$ mice.

(G) Representative image of TA motor neurons at L2 level retrogradely labeled by injection of CTB-647 into the TA muscle and motor neurons transsynaptically labeled after RVΔG-GFP-EnvA injection into the LG muscle of *Avil::cre*$^{+/-}$; *RGT*$^{+/-}$ mice.

(H) Representative image of TA motor neurons at L3 level retrogradely labeled by injection of CTB-647 into the TA muscle and motor neurons transsynaptically labeled after RVΔG-GFP-EnvA injection into the LG muscle of *Avil::cre*$^{+/-}$; *RGT*$^{+/-}$ mice.

(I) Percentage of TA motor neurons transsynaptically labeled after RVΔG-GFP-EnvA injection into the LG muscle of *Avil::cre*$^{+/-}$; *RGT*$^{+/-}$ mice.

Values in (F) and (I) show mean ± SEM. Scale bars represent 30 μm in (D), (E), (G), and (H). To see related data examining axoaxonic transfer of RV, see Figure S4.

detected GFP^{+} proprioceptors, defined by PV and Runx3 coexpression (de Nooij et al., 2013; Figures 5G–5I). These findings suggest that V0$_C$ interneurons receive sensory input from a subset of PV^{+} nonproprioceptive mechanoreceptors (de Nooij et al., 2013).

We probed the degree to which anterograde transsynaptic transfer is a feature of sensory but not CNS neurons through an analysis of V0$_C$ neuron connectivity. Upon RV transsynaptic tracing from V0$_C$ neurons in *Pitx2::cre* $^{+/-}$; *RGT* $^{+/-}$ mice, we failed to observe GFP-labeled motor neurons, despite the detection of numerous GFP-positive C bouton contacts with motor neurons, identified by apposition of the presynaptic marker vAChT and postsynaptic connexin-32 immunoreactivity (Nagy et al., 1993; Figure 5J). These findings confirm that RV is not transported anterogradely by CNS neurons.

Anterograde RV Transfer Is a General Feature of Sensory Neurons

We also explored whether the anterograde transfer of RV from somatosensory neurons is a specialized property of this neuronal class or a feature common to all primary sensory neurons. We examined RV infection and transfer from olfactory and vestibular sensory neurons to capture the diversity of sensory subtypes, as defined by developmental origin, anatomical organization, and function.

We used *PV::cre* mice to direct RV-G and TVA expression to vestibular sensory neurons (VSNs; Kevetter and Leonard, 2002). After injection of RVΔG-GFP-EnvA into the vestibular labyrinth of neonatal animals, we detected GFP expression in VSNs, as well as in neurons located in known vestibular targets—the nodulus and flocculus in the cerebellum and the

(K and K′) GFP^{+}, ChAT^{+}, NeuN^{+} motor neurons in the spinal cord after injection of RVΔG-GFP-EnvA in *PV::cre*$^{+/-}$; *RGT*$^{+/-}$ animals.

(L) Quantitation of NeuN expression levels and motor neuron soma area of GFP^{+} neurons after RVΔG-GFP-EnvA muscle injection in *PV::cre*$^{+/-}$; *RGT*$^{+/-}$ animals.

(M and M′) GFP^{+}, ChAT^{+}, Err3^{-} motor neurons in the spinal cord after RVΔG-GFP-EnvA muscle injection in *PV::cre*$^{+/-}$; *RGT*$^{+/-}$ animals.

(N) Quantitation of Err3 levels and motor neuron soma area of GFP^{+} neurons after RVΔG-GFP-EnvA muscle injection in *PV::cre*$^{+/-}$; *RGT*$^{+/-}$ animals.

f.i., fluorescence intensity. Error bars in (D) represent ± SEM. Scale bars represent 20 μm in (F) and (H) and 30 μm in (C), (K), and (M).

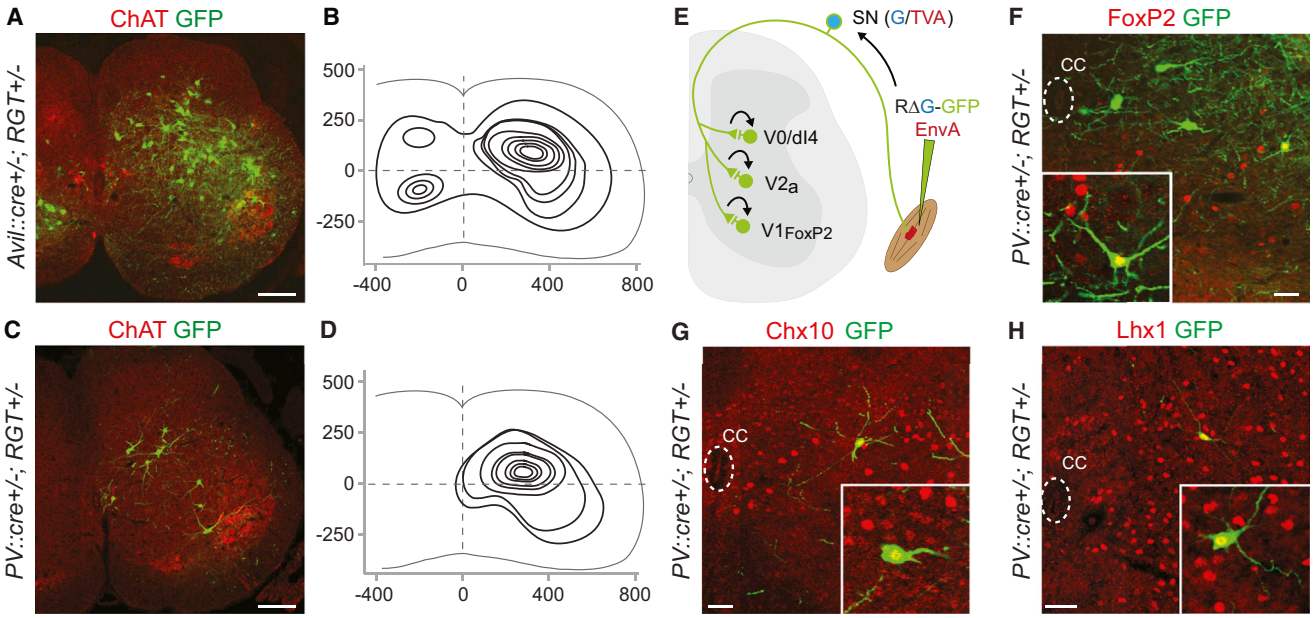

Figure 4. RV Anterograde Transfer Identifies Sensory-Recipient Interneurons

(A) Representative image of GFP$^+$ spinal interneurons labeled by transsynaptic transfer after RVΔG-GFP-EnvA injection into the GS muscle of *Avil::cre*$^{+/-}$; *RGT*$^{+/-}$ animals.

(B) Contour density plot showing the distribution of postsensory interneurons labeled by injection of RVΔG-GFP-EnvA into the GS muscle of *Avil::cre*$^{+/-}$; *RGT*$^{+/-}$ animals. Coordinates are distance in micrometers relative to the central canal.

(C) Representative image of GFP$^+$ spinal interneurons labeled by transsynaptic transfer after RVΔG-GFP-EnvA injection into the GS muscle of *PV::cre*$^{+/-}$; *RGT*$^{+/-}$ animals.

(D) Contour density plot showing the distribution of postsensory interneurons labeled after injection of RVΔG-GFP-EnvA into the GS muscle of *PV::cre*$^{+/-}$; *RGT*$^{+/-}$ animals. Coordinates are distance in micrometers relative to the central canal.

(E) Schematic depicting labeling of defined interneuron classes in the spinal cord by anterograde transsynaptic tracing in *PV::cre*$^{+/-}$; *RGT*$^{+/-}$ animals.

(F) Representative images of FoxP2$^+$ interneurons labeled from transsynaptic transfer from PV$^+$ sensory afferents.

(G) Chx10$^+$ (V2a) interneurons labeled from transsynaptic transfer from PV$^+$ sensory afferents.

(H) Lhx1$^+$ (V0/dI4) interneuron labeled from transsynaptic transfer from PV$^+$ sensory afferents.

Insets in (F), (G), and (H) show additional example of each cell type. cc, central canal. Scale bars represent 50 μm in (A) and (C) and 30 μm in (F), (G), and (H).

vestibular nuclei in the medulla (Figures 6A and 6B and data not shown; Maklad et al., 2010). In the vestibular nuclei, we observed labeled neurons within the superior, medial, and lateral nuclei (Figures 6B and 6C). We also observed GFP$^+$ terminals at lumbar levels in the ventral spinal cord, consistent with the descending projection of the lateral vestibular nucleus (Figure 6D; Liang et al., 2013). In contrast, GFP expression was not detected in ChAT$^+$ putative vestibular efferent neurons located in the medial vestibular nucleus that lack parvalbumin expression (Figure 6B). These findings show that primary VSNs transfer RV transsynaptically through an anterograde route to infect vestibular sensory-recipient neurons.

Finally, we explored whether olfactory sensory neurons (OSNs) are capable of SAD-B19 RV anterograde transport, as previously suggested for a more virulent wild-type RV strain (Lafay et al., 1991; Astic et al., 1993). Inoculation of RVΔG-GFP in wild-type or *RGT*$^{+/-}$ mice resulted in effective labeling of OSN axons in the glomeruli without infection of postsynaptic targets (Figure S5). We took advantage of the selective expression of the olfactory marker protein (OMP) in OSNs to drive TVA and RV-G expression (Figure 6E; Eggan et al., 2004). We performed unilateral inoculation of RVΔG-GFP-EnvA into the nasal cavity of *OMP-Cre*$^{+/-}$; *RGT*$^{+/-}$ mice. In the olfactory bulb, extensive expression of GFP was detected in mitral, tufted, and periglomerular neurons, known OSN targets (Figures 6F–6H). In addition, we observed sparse labeling of neurons in the granule cell layer, which may reflect OSN transient axonal projection in the granule cell layer (Santacana et al., 1992; Ekberg et al., 2011). These projections are observed up to postnatal day 16, raising the possibility of direct RV transfer between OSNs and neurons in the granule layer (Santacana et al., 1992; Ekberg et al., 2011).

Thus, in all the three sensory systems examined, we detect anterograde transsynaptic transfer of RV, suggesting that this property is common to sensory neurons independent of their developmental provenance and function.

DISCUSSION

The selectivity of sensory modality and the constancy of perception imply a precise logic to the engagement of second-order sensory-recipient neurons—but the underpinnings of such organization remain uncharted in many regions of the

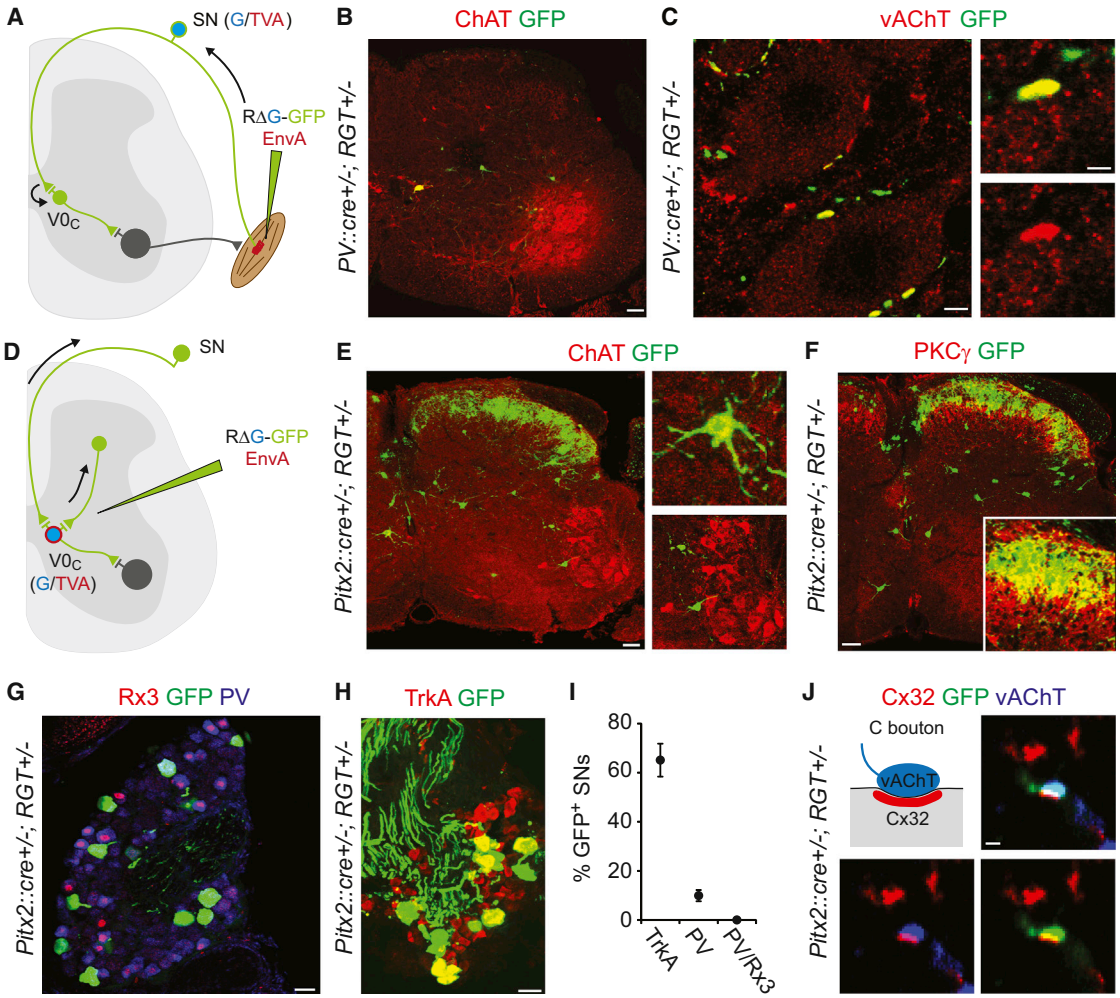

Figure 5. RV Anterograde and Retrograde Transfer Reveals V0C Input/Output Connectivity

(A) Schematic showing anterograde transsynaptic tracing from PV$^+$ sensory neurons and labeling of V0$_C$ interneurons.

(B) Representative image of a GFP$^+$/ChAT$^+$ V0$_C$ interneuron after RV transsynaptic transfer from PV$^+$ sensory neurons.

(C) GFP$^+$/vAChT$^+$ C boutons apposed to motor neuron cell bodies; insets show higher magnification.

(D) Schematic depicting monosynaptic retrograde tracing strategy from V0$_C$ interneurons.

(E) Representative image showing GFP$^+$ interneurons in the lumbar spinal cord. Insets show higher magnification of RV infected V0$_C$ interneuron (top) and ventral horn of spinal cord in same experiments (bottom).

(F) Identification of laminae II/III by PKCγ immunostaining shows that the majority of spinal interneuron inputs to V0c are located dorsal to laminae III.

(G) Representative image of Runx3 and PV status of DRG sensory neurons retrogradely infected from V0$_C$ interneurons.

(H) Representative image of TrkA status of DRG sensory neurons retrogradely infected from V0$_C$ interneurons.

(I) Analysis of TrkA, PV, and PV/Runx3 expression in GFP$^+$ sensory neurons retrogradely infected from V0$_C$ interneurons. Values show mean ± SEM.

(J) Identification of GFP$^+$ C boutons apposed to motor neurons by colabeling with the presynaptic marker vAChT and the postsynaptic marker connexin-32 (Nagy et al., 1993). Scale bars represent 50 μm in (B), (E), (F), (G), and (H) and 2 μm (C) and (J).

CNS. In this study, we outline one strategy for defining sensory-recipient neurons and their connections, through the anterograde transsynaptic transfer of rabies virus. One feature of anterograde transfer to sensory-recipient neurons is the ability to correlate sensory input modality with output connectivity to third-order neurons. Along the way, our findings question two preconceptions of applied rabies virus biology: the lack of infection of primary sensory neurons and the exclusivity of retrograde viral transfer.

Sensory Circuit Mapping through Anterograde Transsynaptic Transfer

In principle, the transsynaptic transfer of RV to sensory-recipient neurons offers a general method for delineating the cohort of second-order neurons involved in the central processing of sensory signals. In the somatosensory system, recent studies have indicated that primary sensory neurons conveying different modalities possess distinct molecular signatures (Marmigère and Ernfors, 2007; Abraira and Ginty, 2013). Thus, anterograde

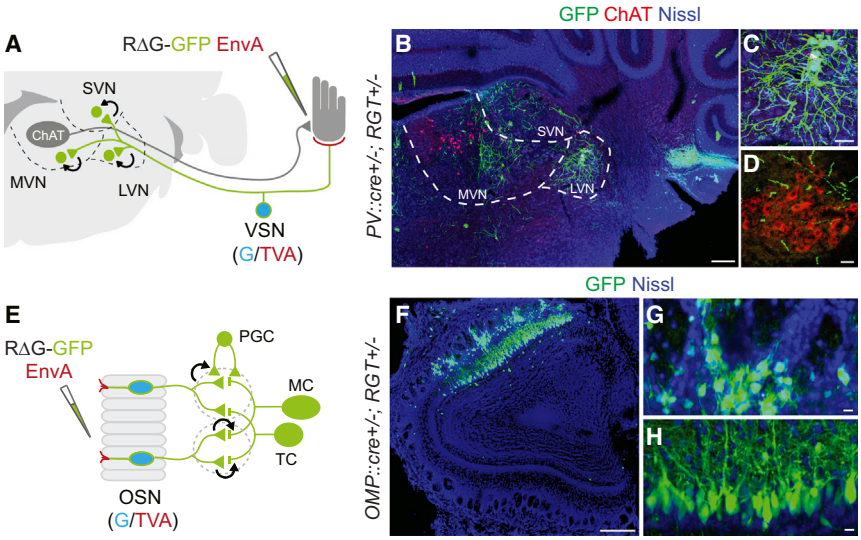

Figure 6. Anterograde Transsynaptic Transfer of RV from Vestibular and Olfactory Sensory Neurons

(A) Schematic depicting anterograde transsynaptic transport from vestibular sensory neurons (VSNs).

(B) Representative image of GFP$^+$ neurons in the medial, superior, and lateral vestibular nuclei (MVN, SVN, and LVN, respectively).

(C) Higher-magnification image of neurons in the lateral vestibular nucleus.

(D) Representative image of the ventral horn of the lumbar spinal cord showing GFP$^+$ axons nearby ChAT$^+$ motor neurons.

(E) Schematic depicting strategy for anterograde transsynaptic tracing from olfactory sensory neurons (OSNs).

(F) Representative image of the olfactory bulb showing anterogradely infected GFP$^+$ neurons.

(G) High-magnification image of GFP$^+$ periglomerular cells (PGCs).

(H) High-magnification image of GFP$^+$ mitral (MC) and tufted (TC) cells. Scale bars represent 250 μm in (B) and (F) and 30 μm in (C), (D), (G), and (H).

To see related data examining OSN axon terminals in the olfactory bulb, see Figure S5.

viral tracing offers the promise of a complete description of the organization of modality-constrained sensory-recipient neurons. The ease of modification of the RV genome also permits expression of proteins that facilitate neural circuit mapping, as well as the interrogation and perturbation of neuronal activity patterns (Osakada et al., 2011; Osakada and Callaway, 2013).

The distribution of proprioceptive sensory-recipient neurons in the spinal cord revealed by RV transsynaptic tracing is consistent with the known trajectory and termination of proprioceptive afferents (Brown, 1981). The distribution of interneurons labeled by anterograde sensory transfer also exhibits significant overlap with the location of premotor interneurons marked by motor neuron retrograde transfer of RV (Stepien et al., 2010; Tripodi et al., 2011). The positional overlap and potential coincidence of these two populations could be accounted for by the fact that certain spinal premotor interneurons also receive direct proprioceptive input and thus would serve as intermediaries in conveying feedforward information from sensory to motor neurons.

Prior studies in which retrograde RV transsynaptic transfer has been used to map premotor interneurons have left unresolved the question of a contribution of anterograde sensory transfer (Stepien et al., 2010; Tripodi et al., 2011). Our findings do not undermine the conclusions of these prior studies, but they do indicate a general need for caution in mapping and interpreting the organization of sensory-motor circuits on the basis of transsynaptic RV transfer. Rigorous exclusion of the possibility that spinal interneurons classified as premotor have been labeled by anterograde transfer from a sensory neuronal source requires information on the occurrence and selectivity of RV infection and RV-G expression by sensory neurons. Our studies, and those of others (Velandia et al., 2007; Velandia-Romero et al., 2013), document the propensity of sensory neurons, including proprioceptors, for infection by RV. In turn, these findings raise the issue of the degree of sensory tropism achieved with different experimental protocols. We find DRG neuronal infection with both SAD-B19-G and EnvA-pseudotyped RV, consolidating the idea that DRG neurons are naturally susceptible to RV infection. Is it possible then that restrictions in sensory neuronal RV-G determine the extent of anterograde transsynaptic transfer? Several means of achieving RV-G complementation have been used in different studies. In our experiments, RV-G is expressed in sensory neurons under genetic control. In contrast, prior premotor mapping studies have relied on AAV-transduced RV-G complementation after muscle injection (Stepien et al., 2010; Tripodi et al., 2011). We note that many different AAV serotypes infect DRG neurons, including proprioceptors (data not shown and Towne et al., 2009; Mason et al., 2010), an indication that RV-G is likely to be efficiently expressed in sensory neurons. Thus, the cellular and molecular basis of the different specificities of DRG sensory neuronal infection and transsynaptic transfer achieved under different experimental protocols remains unclear.

In principle, anterograde transsynaptic transfer can be used to elucidate several features of the organization of sensory-recipient circuits. RV anterograde transsynaptic transfer not only reveals sensory-recipient neurons but also permits identification of third-order neurons through the analysis of labeled synaptic terminals (Figure 7A). This strategy has revealed the synaptic output of $V0_C$ and lateral vestibular neurons onto spinal target neurons. The combination of selective infection of different sensory subtypes with RV variants expressing distinct fluorophores should permit an analysis of the convergence and divergence of modality-specific sensory neurons to second-order CNS neurons (Figure 7B). This method, for example, could prove useful in defining the identity of wide dynamic range neurons in the dorsal horn of the spinal cord (Leem et al., 1994). In addition, combining anterograde tracing from sensory neurons with retrograde tracing from CNS neurons should make it possible to isolate discrete subpopulations of sensory-recipient neurons

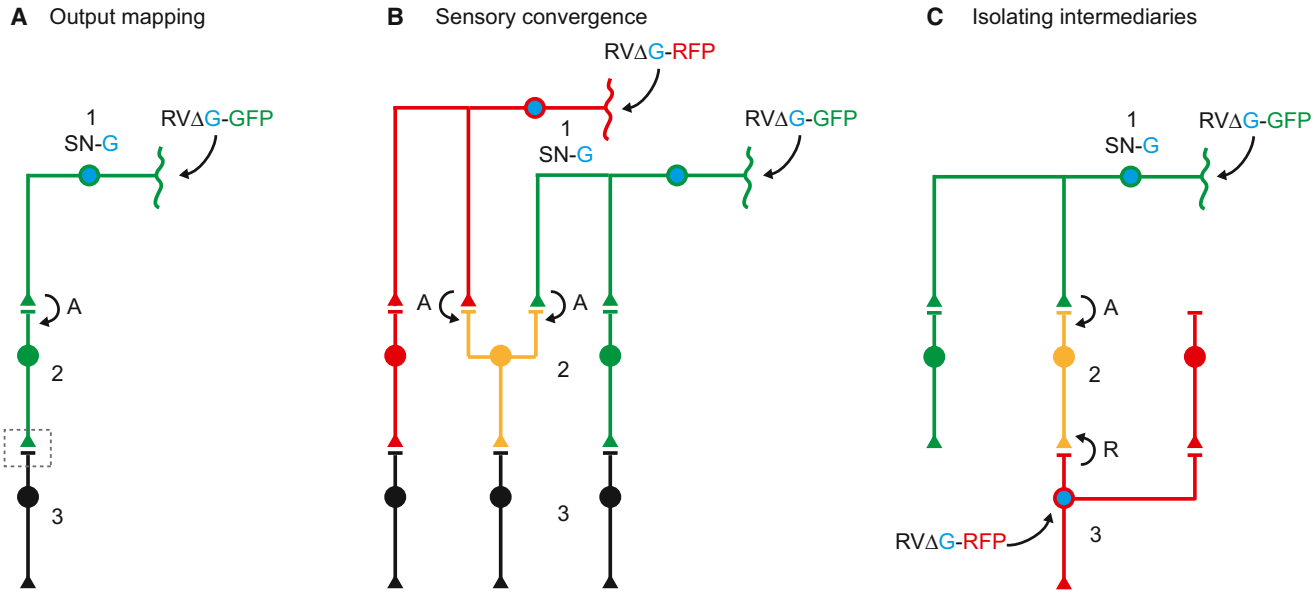

Figure 7. Strategies for Sensory Circuit Mapping Using Anterograde RV Transsynaptic Transfer

(A) RV infection of primary sensory neurons (1) and anterograde ("A") transport into sensory-recipient neurons (2) allows visualization of synaptic inputs to third-order neurons (3).

(B) Dual-color anterograde tracing from different primary sensory neuron populations permits analysis of convergent input to single sensory-recipient neurons.

(C) Combination of anterograde transport from sensory neurons with retrograde ("R") tracing from central neurons permits isolation of intervening second-order neurons.

(Figure 7C). Selective retrograde and anterograde transfer from motor and sensory neurons, for example, should be able to resolve exactly which spinal interneurons serve as single-step intermediaries in the transformation of sensory input to motor output. Although the efficiency of RV coinfection could be limited by viral interference, there is a period when both viral genomes can be replicated, and a recent study describes effective neuronal colabeling using two RVs expressing different reporters, supporting the feasibility of double RV-labeling approaches (Takatoh et al., 2013).

The analysis of $V0_C$ interneurons provides one illustration of the utility of RV tracing methods. We find evidence of direct input from PV^+ sensory neurons to $V0_C$ neurons, an observation that needs to be reconciled with electrophysiological evidence arguing for a lack of direct proprioceptive input to these interneurons (Witts et al., 2014). The combined use of anterograde and retrograde RV tracing shows that direct sensory inputs to $V0_C$ neurons originate from a small nonproprioceptive subpopulation of PV^+ mechanoreceptors (de Nooij et al., 2013). Moreover, $V0_C$ interneurons receive monosynaptic input from nociceptive sensory neurons as well as input from interneurons in laminae II/III that are known to be involved in nociceptive sensory processing (Lallemend and Ernfors, 2012). Taken together, these data suggest a role for $V0_C$ neurons as integrators of low- and high-threshold sensory modalities.

Rabies Virus Infection and Transport in Sensory and Central Neurons

Our work has relevance to two aspects of the application of RV in circuit mapping: the ambiguous tropism for sensory neurons and the directional selectivity of transsynaptic transfer. The ability of RV to infect sensory neurons has not been thoroughly tested, although several studies have indicated that sensory neurons of primates, rats, and guinea pigs are not susceptible to infection (Ugolini, 2011). Nevertheless in mice, wild-type RV has been reported to infect motor neurons and sensory neurons with equal efficiency (Coulon et al., 1989). Our experiments show that the attenuated SAD-B19 strain of RV can infect multiple sensory neuron subtypes in the DRG, as well as sensory neurons in the vestibular and olfactory systems, with no inherent restriction in sensory neuronal subtype tropism.

It is intriguing that the directionality of RV transsynaptic transfer differs in central and sensory neurons. This feature has also been observed in other virus families. Strains of herpes simplex virus (HSV) that are transsynaptically transported in the anterograde direction in the CNS (i.e., H129) can be transported retrogradely from the periphery in sensory neurons (Song et al., 2009). Additionally, pseudorabies virus (PRV) Bartha travels transsynaptically in the retrograde direction in the CNS but has the capacity for anterograde transsynaptic transfer in sensory neurons (Card et al., 1997). The bidirectional transport of HSV has been linked to its ability to interact with both kinesin and dynein classes of molecular motors (Zaichick et al., 2011). Although the cellular and molecular basis of transport is not well understood, RV is believed to be actively transported along microtubules (Klingen et al., 2008) and is capable of interacting with dynein family members (Raux et al., 2000; Jacob et al., 2000), suggesting a similar mechanism for retrograde movement. The direction of RV transport may therefore be dictated by differences in molecular motors and cytoskeletal dynamics in sensory and CNS neurons.

A critical feature of retrograde RV tracing has been exclusive transfer through synaptic connections, permitting unambiguous identification of interconnected neurons (Iwasaki and Clark, 1975; Charlton and Casey, 1979; Dum and Strick, 2013). Our studies imply that anterograde transfer also occurs exclusively via synaptic mechanisms, as shown by the observation that RV infection from proprioceptive neurons is restricted only to motor neurons receiving monosynaptic input. These findings, in turn, raise the issue of whether RV uses similar strategies for release at synaptic terminals and dendrites. Unlike the retrograde spreading of rabies virus in the CNS, where transfer proceeds from somatodendritic compartment to presynaptic terminals, both the axodendritc and the axoaxonic routes could potentially be used to achieve anterograde transfer. Our results indicate that RV is indeed transferred via axodendritic and/or axosomatic synapses to motor neurons. Axoaxonic synapses also appear to be a substrate for anterograde RV transfer. In preliminary experiments, we have found infection of GABApre interneurons whose axoaxonic boutons mediate presynaptic inhibition of proprioceptive input to motor neurons.

Regardless of the molecular mechanism of directional transfer and synaptic release, our observations reveal that somatosensory, vestibular, and olfactory sensory neurons are each capable of conveying anterograde RV transsynaptic transfer. Anterograde RV transfer may therefore be a feature of all classes of primary sensory neurons, independent of their developmental origin and function, opening the way for a systematic analysis of CNS circuits engaged by different sensory modalities.

EXPERIMENTAL PROCEDURES

Mouse Strains

PV::cre (Hippenmeyer et al., 2007), *Avil::cre* (da Silva et al., 2011), RGT (Takatoh et al., 2013), *OMP::cre* (Eggan et al., 2004), *ROSA-loxP-STOP-loxP-tdTomato* (Ai14; Madisen et al., 2010), and *Pitx2::cre* (Liu et al., 2003) have been described. All experiments were performed according to Columbia University guidelines.

In Situ Hybridization

In situ hybridization was performed on 15–20 μm cryostat sections using digoxigenin (DIG)-labeled probes (Demireva et al., 2011). Probes for rabies B19 glycoprotein were generated by PCR from cDNA using the following probe sequences: forward: 5′-CCTGGGTTTGGAAAAGCATA-3′, reverse: 5′-GCGCTAATACGACTCACTATAGGGAGGGATGATTGCATCTCTGG-3′.

Production of Glycoprotein-Deficient Rabies Virus

RVΔG-GFP was produced as described in Wickersham et al. (2010) and Osakada and Callaway (2013) with minor modifications. B7GG cells were transfected with 36 μg pSAD-ΔG-GFP, 18 μg pSAD-B19N, 9 μg pSAD-B19P, 9 μg pSAD-B19L, and 7.2 μg pSAD-B19G. Viral particles were harvested and propagated by further infection of B7GG cells in a Corning cell farm. Virus was concentrated via ultracentrifugation, resuspended in PBS, and further concentrated in Amicon Ultra 100 kDa protein concentrators (Millipore) to achieve a viral titer of 1×10^{11} infectious particles per milliliter as assayed by serial dilutions of virus onto HEK293 cells.

Production of EnvA-Pseudotyped Glycoprotein-Deficient Rabies Virus

RVΔG-GFP-EnvA was produced essentially as described in Wickersham et al. (2010) with minor modifications. BHK-EnvA cells were infected with RVΔG-GFP at a multiplicity of infection (MOI) of 2. Twenty-four hours later, cells were washed three times in PBS and fresh media added, and this was repeated 24 hr later. After a subsequent 48 hr incubation, media was harvested and filtered and viral particles were concentrated by centrifugation. The virus was resuspended in PBS and further concentrated in Amicon Ultra 100 kDa protein concentrators. Viral titer was assessed by serial dilution of the virus on HEK293-TVA cells (Wickersham et al., 2010), and virus of titer 1×10^9 used for inoculation.

Inoculation of Rabies Virus

For rabies tracing experiments, wild-type and mutant mice at postnatal day 4 were anesthetized with 4% isofluorane in oxygen and 2 μl of RVΔG-GFP-EnvA or RVΔG-GFP was inoculated with a glass capillary into either the GS or TA muscle for analysis of somatosensory system, in the nostril for analysis of the olfactory system, and in the vestibular labyrinth for analysis of the vestibular system. To retrogradely label motor neurons, we injected about 10–50 nl of 1% solution of Alexa-conjugated CTB (Life Technologies) into the MG or TA muscles. Animals were sacrificed 3 to 6 days later by transcardial perfusion with PBS followed by 4% paraformaldehyde in phosphate buffer.

Immunohistochemistry

Tissue was cryoprotected in 30% sucrose in phosphate buffer, frozen in optimal cutting temperature compound, and sectioned at 40 μm on a Leica cryostat. Sections were processed as described previously (Demireva et al., 2011). Antibodies used in this study were as follows: goat anti-GFP and chicken anti-GFP (both Abcam), rabbit anti-ChAT (Demireva et al., 2011), mouse anti-NeuN (Chemicon), mouse anti-Err3 (PPMX), goat anti-CTB (List Laboratories), chicken anti-PV (de Nooij et al., 2013), rabbit anti-Runx3 (Kramer et al., 2006), goat anti-FoxP2 (Santa-Cruz Biotechnology), mouse anti-connexin-32 (Nagy et al., 1993), rabbit anti-Chx10 (Pierani et al., 2001), rabbit anti-Lhx1 (Kania et al., 2000), rabbit anti-GAD2 (Betley et al., 2009), and rabbit anti-TrkA (a generous gift from Dr. L. Reichardt).

Motor and Interneuron Position Analysis

We acquired z stack images to cover the entire thickness of the sections using a Zeiss 510 laser-scanning confocal microscope. The position of each neuron was analyzed using the cell counter function in ImageJ (National Institutes of Health) and three-dimensional coordinates calculated relative to the central canal. Contour distributions were calculated and plotted in "R project" (R foundation for statistical computing, Vienna, Austria; http://www.r-project.org).

SUPPLEMENTAL INFORMATION

Supplemental Information includes Supplemental Experimental Procedures and five figures and can be found with this article online at http://dx.doi.org/10.1016/j.neuron.2013.12.033.

ACKNOWLEDGMENTS

We would like to thank Benjamin Arenkiel (Baylor College of Medicine) for generously providing the RGT mouse line and Fan Wang (Duke University) for the Advillin::cre mouse line; Edward Callaway (Salk Institute) for SAD-B19 plasmids (Addgene plasmids 32630, 32631, 32632, 32633, 32635) and the BHK-EnvA, B7GG, and HEK293-TVA cell lines; Thomas Reardon for advice and help with viral techniques; Kevin Franks for advice on olfactory system experiments; Qiaolian Liu, Staceyann Doobar, and Daniel Martin for technical assistance; Joriene de Nooij and Amy Norovich for providing counts of GTO/muscle spindles; and Joriene de Nooij for discussions on sensory neuron biology. We are grateful to Silvia Arber, Jay Bikoff, Joriene de Nooij, and Thomas Reardon for comments on the manuscript. T.M.J. was supported by NIH grant NS0332245 and Project A.L.S. T.M.J. is an HHMI investigator.

Accepted: December 16, 2013
Published: January 30, 2014

REFERENCES

Abraira, V.E., and Ginty, D.D. (2013). The sensory neurons of touch. Neuron *79*, 618–639.

Al-Mosawie, A., Wilson, J.M., and Brownstone, R.M. (2007). Heterogeneity of V2-derived interneurons in the adult mouse spinal cord. Eur. J. Neurosci. *26*, 3003–3015.

Ashrafi, S., Lalancette-Hébert, M., Friese, A., Sigrist, M., Arber, S., Shneider, N.A., and Kaltschmidt, J.A. (2012). Wnt7A identifies embryonic γ-motor neurons and reveals early postnatal dependence of γ-motor neurons on a muscle spindle-derived signal. J. Neurosci. *32*, 8725–8731.

Astic, L., Saucier, D., Coulon, P., Lafay, F., and Flamand, A. (1993). The CVS strain of rabies virus as transneuronal tracer in the olfactory system of mice. Brain Res. *619*, 146–156.

Betley, J.N., Wright, C.V., Kawaguchi, Y., Erdélyi, F., Szabó, G., Jessell, T.M., and Kaltschmidt, J.A. (2009). Stringent specificity in the construction of a GABAergic presynaptic inhibitory circuit. Cell *139*, 161–174.

Boehm, U., Zou, Z., and Buck, L.B. (2005). Feedback loops link odor and pheromone signaling with reproduction. Cell *123*, 683–695.

Braz, J.M., Rico, B., and Basbaum, A.I. (2002). Transneuronal tracing of diverse CNS circuits by Cre-mediated induction of wheat germ agglutinin in transgenic mice. Proc. Natl. Acad. Sci. USA *99*, 15148–15153.

Brown, A.G. (1981). Organization in the Spinal Cord: the Anatomy and Physiology of Identified Neurones. (Berlin: Springer).

Burke, R.E., and Tsairis, P. (1973). Anatomy and innervation ratios in motor units of cat gastrocnemius. J. Physiol. *234*, 749–765.

Burke, R.E., Strick, P.L., Kanda, K., Kim, C.C., and Walmsley, B. (1977). Anatomy of medial gastrocnemius and soleus motor nuclei in cat spinal cord. J. Neurophysiol. *40*, 667–680.

Callaway, E.M. (2008). Transneuronal circuit tracing with neurotropic viruses. Curr. Opin. Neurobiol. *18*, 617–623.

Card, J.P., Enquist, L.W., Miller, A.D., and Yates, B.J. (1997). Differential tropism of pseudorabies virus for sensory neurons in the cat. J. Neurovirol. *3*, 49–61.

Charlton, K.M., and Casey, G.A. (1979). Experimental rabies in skunks: immunofluorescence light and electron microscopic studies. Lab. Invest. *41*, 36–44.

Coulon, P., Derbin, C., Kucera, P., Lafay, F., Prehaud, C., and Flamand, A. (1989). Invasion of the peripheral nervous systems of adult mice by the CVS strain of rabies virus and its avirulent derivative AvO1. J. Virol. *63*, 3550–3554.

da Silva, S., Hasegawa, H., Scott, A., Zhou, X., Wagner, A.K., Han, B.X., and Wang, F. (2011). Proper formation of whisker barrelettes requires periphery-derived Smad4-dependent TGF-beta signaling. Proc. Natl. Acad. Sci. USA *108*, 3395–3400.

de Nooij, J.C., Doobar, S., and Jessell, T.M. (2013). Etv1 inactivation reveals proprioceptor subclasses that reflect the level of NT3 expression in muscle targets. Neuron *77*, 1055–1068.

Demireva, E.Y., Shapiro, L.S., Jessell, T.M., and Zampieri, N. (2011). Motor neuron position and topographic order imposed by β- and γ-catenin activities. Cell *147*, 641–652.

Dum, R.P., and Strick, P.L. (2013). Transneuronal tracing with neurotropic viruses reveals network macroarchitecture. Curr. Opin. Neurobiol. *23*, 245–249.

Eccles, R.M., and Lundberg, A. (1958). Integrative pattern of Ia synaptic actions on motoneurones of hip and knee muscles. J. Physiol. *144*, 271–298.

Eccles, J.C., Eccles, R.M., and Lundberg, A. (1957). The convergence of monosynaptic excitatory afferents on to many different species of alpha motoneurones. J. Physiol. *137*, 22–50.

Eccles, J.C., Eccles, R.M., Iggo, A., and Lundberg, A. (1960). Electrophysiological studies on gamma motoneurones. Acta Physiol. Scand. *50*, 32–40.

Eggan, K., Baldwin, K., Tackett, M., Osborne, J., Gogos, J., Chess, A., Axel, R., and Jaenisch, R. (2004). Mice cloned from olfactory sensory neurons. Nature *428*, 44–49.

Ekberg, J.A., Amaya, D., Chehrehasa, F., Lineburg, K., Claxton, C., Windus, L.C., Key, B., Mackay-Sim, A., and St John, J.A. (2011). OMP-ZsGreen fluorescent protein transgenic mice for visualisation of olfactory sensory neurons in vivo and in vitro. J. Neurosci. Methods *196*, 88–98.

Friese, A., Kaltschmidt, J.A., Ladle, D.R., Sigrist, M., Jessell, T.M., and Arber, S. (2009). Gamma and alpha motor neurons distinguished by expression of transcription factor Err3. Proc. Natl. Acad. Sci. USA *106*, 13588–13593.

Hippenmeyer, S., Huber, R.M., Ladle, D.R., Murphy, K., and Arber, S. (2007). ETS transcription factor Erm controls subsynaptic gene expression in skeletal muscles. Neuron *55*, 726–740.

Horowitz, L.F., Montmayeur, J.P., Echelard, Y., and Buck, L.B. (1999). A genetic approach to trace neural circuits. Proc. Natl. Acad. Sci. USA *96*, 3194–3199.

Iwasaki, Y., and Clark, H.F. (1975). Cell to cell transmission of virus in the central nervous system. II. Experimental rabies in mouse. Lab. Invest. *33*, 391–399.

Jacob, Y., Badrane, H., Ceccaldi, P.E., and Tordo, N. (2000). Cytoplasmic dynein LC8 interacts with lyssavirus phosphoprotein. J. Virol. *74*, 10217–10222.

Kania, A., Johnson, R.L., and Jessell, T.M. (2000). Coordinate roles for LIM homeobox genes in directing the dorsoventral trajectory of motor axons in the vertebrate limb. Cell *102*, 161–173.

Kevetter, G.A., and Leonard, R.B. (2002). Molecular probes of the vestibular nerve. II. Characterization of neurons in Scarpa's ganglion to determine separate populations within the nerve. Brain Res. *928*, 18–29.

Klingen, Y., Conzelmann, K.K., and Finke, S. (2008). Double-labeled rabies virus: live tracking of enveloped virus transport. J. Virol. *82*, 237–245.

Kramer, I., Sigrist, M., de Nooij, J.C., Taniuchi, I., Jessell, T.M., and Arber, S. (2006). A role for Runx transcription factor signaling in dorsal root ganglion sensory neuron diversification. Neuron *49*, 379–393.

Lafay, F., Coulon, P., Astic, L., Saucier, D., Riche, D., Holley, A., and Flamand, A. (1991). Spread of the CVS strain of rabies virus and of the avirulent mutant AvO1 along the olfactory pathways of the mouse after intranasal inoculation. Virology *183*, 320–330.

Lallemend, F., and Ernfors, P. (2012). Molecular interactions underlying the specification of sensory neurons. Trends Neurosci. *35*, 373–381.

Leem, J.W., Lee, B.H., Willis, W.D., and Chung, J.M. (1994). Grouping of somatosensory neurons in the spinal cord and the gracile nucleus of the rat by cluster analysis. J. Neurophysiol. *72*, 2590–2597.

Liang, H., Bácskai, T., Watson, C., and Paxinos, G. (2013). Projections from the lateral vestibular nucleus to the spinal cord in the mouse. Brain Struct. Funct. Published online March 16, 3013. http://dx.doi.org/10.1007/s00429-013-0536-4.

Liu, W., Selever, J., Lu, M.F., and Martin, J.F. (2003). Genetic dissection of Pitx2 in craniofacial development uncovers new functions in branchial arch morphogenesis, late aspects of tooth morphogenesis and cell migration. Development *130*, 6375–6385.

Madisen, L., Zwingman, T.A., Sunkin, S.M., Oh, S.W., Zariwala, H.A., Gu, H., Ng, L.L., Palmiter, R.D., Hawrylycz, M.J., Jones, A.R., et al. (2010). A robust and high-throughput Cre reporting and characterization system for the whole mouse brain. Nat. Neurosci. *13*, 133–140.

Maklad, A., Kamel, S., Wong, E., and Fritzsch, B. (2010). Development and organization of polarity-specific segregation of primary vestibular afferent fibers in mice. Cell Tissue Res. *340*, 303–321.

Marmigère, F., and Ernfors, P. (2007). Specification and connectivity of neuronal subtypes in the sensory lineage. Nat. Rev. Neurosci. *8*, 114–127.

Mason, M.R., Ehlert, E.M., Eggers, R., Pool, C.W., Hermening, S., Huseinovic, A., Timmermans, E., Blits, B., and Verhaagen, J. (2010). Comparison of AAV serotypes for gene delivery to dorsal root ganglion neurons. Mol. Ther. *18*, 715–724.

Mata, M., Glorioso, J.C., and Fink, D.J. (2002). Targeted gene delivery to the nervous system using herpes simplex virus vectors. Physiol. Behav. *77*, 483–488.

McHanwell, S., and Biscoe, T.J. (1981). The localization of motoneurons supplying the hindlimb muscles of the mouse. Philos. Trans. R. Soc. Lond. B Biol. Sci. *293*, 477–508.

Mendelson, B., and Frank, E. (1991). Specific monosynaptic sensory-motor connections form in the absence of patterned neural activity and motoneuronal cell death. J. Neurosci. *11*, 1390–1403.

Morikawa, Y., Hisaoka, T., and Senba, E. (2009). Characterization of Foxp2-expressing cells in the developing spinal cord. Neuroscience *162*, 1150–1162.

Nagy, J.I., Yamamoto, T., and Jordan, L.M. (1993). Evidence for the cholinergic nature of C-terminals associated with subsurface cisterns in alpha-motoneurons of rat. Synapse *15*, 17–32.

Nelson, S.G., and Mendell, L.M. (1978). Projection of single knee flexor Ia fibers to homonymous and heteronymous motoneurons. J. Neurophysiol. *41*, 778–787.

Osakada, F., and Callaway, E.M. (2013). Design and generation of recombinant rabies virus vectors. Nat. Protoc. *8*, 1583–1601.

Osakada, F., Mori, T., Cetin, A.H., Marshel, J.H., Virgen, B., and Callaway, E.M. (2011). New rabies virus variants for monitoring and manipulating activity and gene expression in defined neural circuits. Neuron *71*, 617–631.

Pierani, A., Moran-Rivard, L., Sunshine, M.J., Littman, D.R., Goulding, M., and Jessell, T.M. (2001). Control of interneuron fate in the developing spinal cord by the progenitor homeodomain protein Dbx1. Neuron *29*, 367–384.

Pillai, A., Mansouri, A., Behringer, R., Westphal, H., and Goulding, M. (2007). Lhx1 and Lhx5 maintain the inhibitory-neurotransmitter status of interneurons in the dorsal spinal cord. Development *134*, 357–366.

Raux, H., Flamand, A., and Blondel, D. (2000). Interaction of the rabies virus P protein with the LC8 dynein light chain. J. Virol. *74*, 10212–10216.

Santacana, M., Heredia, M., and Valverde, F. (1992). Transient pattern of exuberant projections of olfactory axons during development in the rat. Brain Res. Dev. Brain Res. *70*, 213–222.

Smith, C.L. (1983). The development and postnatal organization of primary afferent projections to the rat thoracic spinal cord. J. Comp. Neurol. *220*, 29–43.

Smith, C.L. (1986). Sensory neurons supplying touch domes near the body midlines project bilaterally in the thoracic spinal cord of rats. J. Comp. Neurol. *245*, 541–552.

Song, C.K., Schwartz, G.J., and Bartness, T.J. (2009). Anterograde transneuronal viral tract tracing reveals central sensory circuits from white adipose tissue. Am. J. Physiol. Regul. Integr. Comp. Physiol. *296*, R501–R511.

Stephens, J.A., Reinking, R.M., and Stuart, D.G. (1975). The motor units of cat medial gastrocnemius: electrical and mechanical properties as a function of muscle length. J. Morphol. *146*, 495–512.

Stepien, A.E., Tripodi, M., and Arber, S. (2010). Monosynaptic rabies virus reveals premotor network organization and synaptic specificity of cholinergic partition cells. Neuron *68*, 456–472.

Takatoh, J., Nelson, A., Zhou, X., Bolton, M.M., Ehlers, M.D., Arenkiel, B.R., Mooney, R., and Wang, F. (2013). New modules are added to vibrissal premotor circuitry with the emergence of exploratory whisking. Neuron *77*, 346–360.

Towne, C., Pertin, M., Beggah, A.T., Aebischer, P., and Decosterd, I. (2009). Recombinant adeno-associated virus serotype 6 (rAAV2/6)-mediated gene transfer to nociceptive neurons through different routes of delivery. Mol. Pain *5*, 52.

Tripodi, M., Stepien, A.E., and Arber, S. (2011). Motor antagonism exposed by spatial segregation and timing of neurogenesis. Nature *479*, 61–66.

Ugolini, G. (2008). Use of rabies virus as a transneuronal tracer of neuronal connections: implications for the understanding of rabies pathogenesis. Dev. Biol. (Basel) *131*, 493–506.

Ugolini, G. (2010). Advances in viral transneuronal tracing. J. Neurosci. Methods *194*, 2–20.

Ugolini, G. (2011). Rabies virus as a transneuronal tracer of neuronal connections. Adv. Virus Res. *79*, 165–202.

Velandia, M.L., Pérez-Castro, R., Hurtado, H., and Castellanos, J.E. (2007). Ultrastructural description of rabies virus infection in cultured sensory neurons. Mem. Inst. Oswaldo Cruz *102*, 441–447.

Velandia-Romero, M.L., Castellanos, J.E., and Martínez-Gutiérrez, M. (2013). In vivo differential susceptibility of sensory neurons to rabies virus infection. J. Neurovirol. *19*, 367–375.

Wickersham, I.R., Finke, S., Conzelmann, K.K., and Callaway, E.M. (2007a). Retrograde neuronal tracing with a deletion-mutant rabies virus. Nat. Methods *4*, 47–49.

Wickersham, I.R., Lyon, D.C., Barnard, R.J.O., Mori, T., Finke, S., Conzelmann, K.-K., Young, J.A.T., and Callaway, E.M. (2007b). Monosynaptic restriction of transsynaptic tracing from single, genetically targeted neurons. Neuron *53*, 639–647.

Wickersham, I.R., Sullivan, H.A., and Seung, H.S. (2010). Production of glycoprotein-deleted rabies viruses for monosynaptic tracing and high-level gene expression in neurons. Nat. Protoc. *5*, 595–606.

Witts, E.C., Zagoraiou, L., and Miles, G.B. (2014). Anatomy and function of cholinergic C bouton inputs to motor neurons. J. Anat. *224*, 52–60.

Zagoraiou, L., Akay, T., Martin, J.F., Brownstone, R.M., Jessell, T.M., and Miles, G.B. (2009). A cluster of cholinergic premotor interneurons modulates mouse locomotor activity. Neuron *64*, 645–662.

Zaichick, S.V., Bohannon, K.P., and Smith, G.A. (2011). Alphaherpesviruses and the cytoskeleton in neuronal infections. Viruses *3*, 941–981.